Supplementary Material on the Methodology Part IV

Final report on connectivity patterns of blackspot seabream

Consultant
Simone Sammartino

FINAL REPORT

July 15, 2019

Project: Transboundary population structure of Sardine, European hake and Blackspot Seabream in the Alboran Sea and adjacent waters: a multidisciplinary approach (TRANSBORAN). Framework: COPEMEDII project.

Job title: Connectivity patterns of Blackspot seabream in the Alboran Sea

Division: Fisheries and Aquaculture Policy and Resources Division (FIA) / Fisheries and Aquaculture Department (FI)

Programme number: GCP/INT/317 EC Year 9

Consultant: Simone Sammartino

Index of contents

1. Introduction

This document provides the final report of the job titled **Connectivity patterns of Blackspot seabream in the Alboran Sea**, assigned to the consultant Simone Sammartino, within the framework of the FAO project **Transboundary population structure of Sardine, European hake and Blackspot Seabream in the Alboran Sea and adjacent waters: a multidisciplinary approach (TRANSBORAN)**. The job aims to assess the connectivity path of the commercially appreciated fish species Blackspot seabream (Pagellus bogaraveo, Brünnich, 1768) in the Strait of Gibraltar – Alboran Sea area (Western Mediterranean), by the simulation of the dispersal patterns of its Early Life Stages (eggs and larvae) - ELS.

In this document the reader will find many references to the previous intermediate report, and it is therefore encouraged to browse that to fully understand the discussion provided in the present one. Nevertheless, a short resume of the former is provided in the next section.

2. Brief resume of intermediate report

This study is entirely based on the analysis of the outcomes of a hydrodynamic numerical model run in a spatial domain spanning from the Gulf of Cádiz to the Alboran Sea, centered in the Strait of Gibraltar. The model grid is curvilinear with an uneven horizontal resolution, maximal in the own Strait (*O*(100 m)), keeping a quite constant value of *O*(1000 m) in the whole Alboran basin (see Figure 1 of the intermediate report).

The model has been run during a period of five months, from December 2004 to April 2005, to fully reproduce the main spawning period of the target species, centered in the first trimester of the year (Gil Herrera, 2006). The model is forced with realistic oceanographic and meteorological datasets to properly reproduce a reliable circulation of the region of interest, including the tidal and sub-tidal variability, spanning from semidiurnal to multi-days frequency.

A detailed analysis of the model outcomes is provided, describing the general circulation pattern and the principal large-scale dynamic structures, such as the Atlantic Jet (AJ) and the Alboran Gyres, the tidal variability, with the strong influence of semidiurnal cycle acting with special intensity in the own Strait, and the subinertial modulation mainly driven by fortnightly tidal cycle (spring-neap cycle) and meteorological forcing (winds and atmospheric pressure).

After describing the main features of the AJ and its direct influence on the shape and size variability of the Western Alboran Gyre (WAG), presenting the evolution from a more coastal small-scale gyre in full winter to a more stable and larger gyre in late spring, few examples of both tidal and subinertial variability are presented. Although tides are the predominant forcing in the Strait, subinertial variability can reach the same order of magnitude of the former, and break the tidal pattern introducing important large scale variations to the circulation scheme.

Last part of the report is addressed to a sensitivity analysis of the Lagrangian Particles Tracking (LPT) algorithm employed in this study, to evaluate the robustness of the method and its reliability in the assessment of the connectivity pattern of the target species in the study region.

3. Job milestones

The main tasks of the job are resumed in the intermediate report and are reported here:

1. Implementation of the numerical model
    a. Implementation of the model (geometry, bathymetry, parameterization)
    b. Gathering of the initial and boundary conditions
    c. Execution of the hydrodynamic model
2. Analysis of the model outcome
3. Sensitivity tests
4. Execution of the LPT algorithm
    a. Release times definition
    b. Execution of the LPT algorithm
5. Statistical processing of the simulated trajectories
6. Interpretation of results

All stages are completed at 100%, whereas only tasks 4-6 will be described in the present document. For further details on the previous tasks, please refer to the intermediate report.

4. LPT experiments

As mentioned in the intermediate report, a Lagrangian Particles Tracking algorithm has been applied to the horizontal current fields to obtain the dispersal patterns of the Early Life Stages (ELS) of the target species, treated as purely passive tracers.

4.1. Temporal variability

In order to assess the effect of the different time-scale forcings described before on the modulation of the particles trajectories, a series of experiments has been executed, with release times ordered over the course of the months of January and February 2005 (Figure 1).

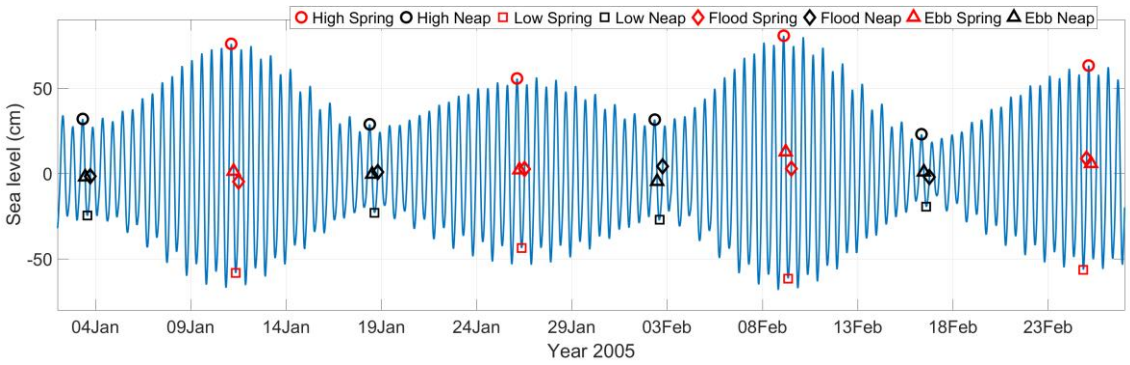

Figure 1 – Sea level of the simulated period (Tarifa) and release times of the experiments executed in the study. See legend for symbols interpretation.

Each experiment lasted 60 days, to fully include the Pelagic Larval Duration (PLD) of the target species that is roughly estimated as 45-60 days (Burgos et al., 2013; Gil Herrera, 2006).

Release times coincide with different combination of tidal phase and tidal fortnightly modulation, being the former classified into high, ebb (from high to low), low and flood (from

low to high) tide, and the latter into spring and neap tide. The combination of both series provides a total of 8 different tidal conditions (see legend in Figure 1). Moreover, in order to obtain some kind of estimate of the uncertainty of the own experiments, driven by the aforementioned large-scale variability, four replicas of each condition have been considered, repeating them over four fortnightly cycles (two months, see Figure 1). Under these circumstances a total of 32 experiments have been implemented to assess the temporal variability of the system dynamics.

4.2. Spatial variability

Once answered the question of "when to release ELS", it is necessary to decide "where" to do it. It is indeed expectable that a great sensitivity of the LPT experiments is due to the choice of the area of release.

Basing on the knowledge of the life cycle of the target species (Báez et al., 2014; Gil and Sobrino, 2002), and after several communications with colleague Juan Gil Herrera from the Spanish Oceanographic Institute, a common concern raises, based on the statement that the Strait of Gibraltar can be considered as the main habitat for adults specimens and hence the principal spawning area.

Following Gil Herrera (2006), adult females, who live in deep waters in the Straits, would raise to the limits of the continental slope to spawn over few hundreds of meters depth, approximately, although any robust observational confirmation of it is still unavailable. With such large degree of uncertainness, a set of three zones have been defined as areas of release (see inset of Figure 2).

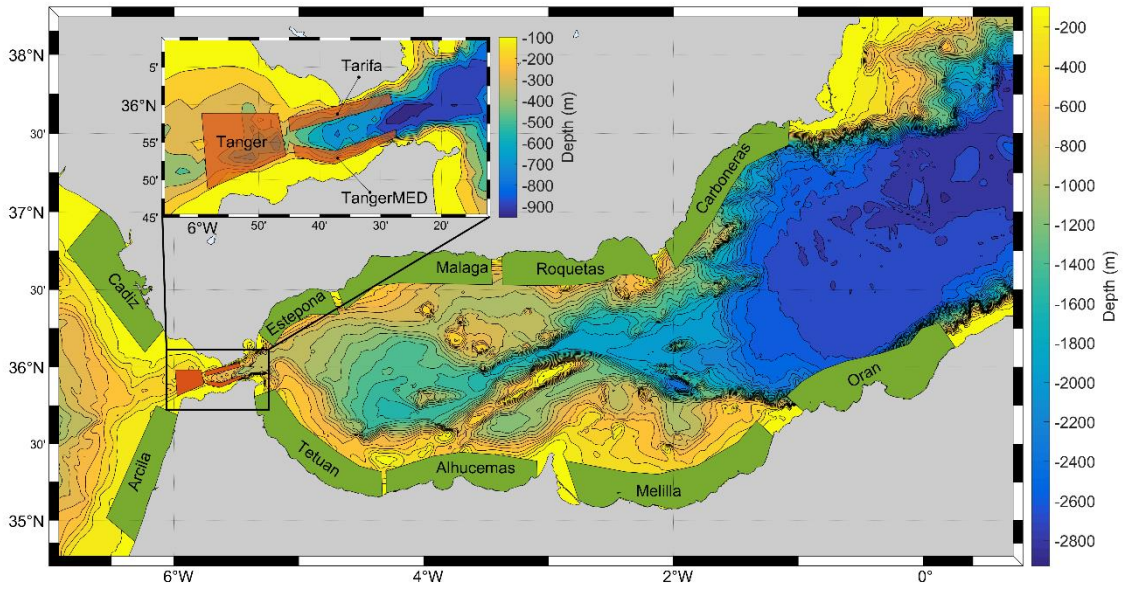

Figure 2 –Release (see also inset) and landing areas, used in the connectivity analysis carried out in this study.

Two of them, Tarifa and TangerMED, are narrow polygons of approximately 25 km length and 3 km width located at the northern and southern limit of the 100 m isobaths, respectively, in the main channel of the Strait, while a third one, Tanger, is a wider polygon of approximately 20 km x 15 km, located at the western margin of the Strait, west of the shallower Camarinal Sill. The sill is expected to be an important barrier for a west-east biological connectivity, and indeed it

is a huge dynamic obstacle from a dynamic point of view, where most of the energy of the Atlantic-Mediterranean waters exchange is dissipated in the Strait (García-Lafuente et al., 2018; Wesson and Gregg, 1994).

The degree of uncertainty of the exact zone of spawning of the target species is equally present in the knowledge of the depth of spawning and on the vertical displacement the ELS are submitted to, actively or passively, throughout their subsequent spread. Hence, a total of 5 different depths distributed through the first 80 m depth approximately (namely 1 m, 12 m, 25 m, 52 m and 81 m depth), have been defined as horizontal layers of the 3D velocity fields to be used as inputs for the ELS trajectories computation.

Both the horizontal area and the vertical depth of release are two further degrees of freedom of the whole matrix of Lagrangian experiments, whose 32 temporal combinations have to be multiplied by three areas of release and by 5 depths of release. All this sums up a total of 480 different experiments, each with a total length of 60 days, and a temporal discretization of 5 minutes (time interval at which particles position is computed). Each experiment consists in releasing a total of ∼1000 particles in one of the corresponding areas of release illustrated in the inset of Figure 2.

4.3. Connectivity computation

Generally, connectivity is assessed by computing the percentage of particles released in area A and located inside area B, after a certain time interval (LaCasce, 2008). Also, generally an inverse connectivity is computed calculating the same percentage from area B to area A. Therefore, a full connectivity matrix C is obtained, in which each element C_{ij} defines the percentage of particles released in area i and collected in area j. The diagonal of this matrix, that is the elements C_{ij}, with $i \equiv j$, are defined as self-connectivity, or self-recruitment. While general connectivity expresses the relative abundance of eggs spawned in a certain area and recruited (development and growth) in another, self-connectivity defines the percentage of individuals that remain in the same region where they have been spawned, and grow there.

As mentioned before, the target species has a specific preference for spawning in the Strait, a highly energetic zone, where self-recruitment is not only unwanted by the own species (larvae and juveniles grow better in low-dynamics conditions), but also mostly prevented by the currents acting there. Therefore, the three release areas defined before are considered as seeding areas only, and the chance of particles to be recollected within those areas (self-recruitment) is not taken into account.

Conversely, the connectivity between the spawning areas in the Strait and the Alboran basin, and secondarily, with the Atlantic Region west of the Strait, are the main objective of this study and are indeed deeply investigated. To this aim, a set of other 10 areas have been defined in the Alboran Sea (8 of them) and in the Gulf of Cádiz and the Atlantic African coast (2 of them, see Figure 2). These areas will be referred here in after to as landing areas. For each of them, the connectivity with one of the release areas is defined as the percentage of particles that are released in one of them and are collected within one of the landing ones.

Figure 3a shows the time series of particles (ELS) released at surface in Tarifa area and collected in Estepona (see Figure 2). The curve shows strong fluctuations of the particles abundance through the first 9 days approximately, and then a quick drop to very low percentages from that

time forward. This behavior is typical of a high energetic system mostly characterized by tidal dynamics. The marked fluctuations of several tens of percentage points, occurring shortly after the release, present a frequency nearly coinciding with the semidiurnal tidal cycle.

For instance, particles position at time 1 (6 days after release, black circles in Figure 3b) shows a bunch of elements bordering with the southern limit of Estepona area, but not entering into it, while only half tidal cycle later (time 2, red circles in Figure 3b) they almost completely invaded the polygon. Notice that those groups of particles depict small-scale cyclonic eddies typical of the filaments detaching from the northern rim of the WAG (see Figure 3 of the intermediate report).

The time series of particles percentages reflects this issue, with values changing from ~5% to 65% in half tidal cycle (see arrows in Figure 3a).

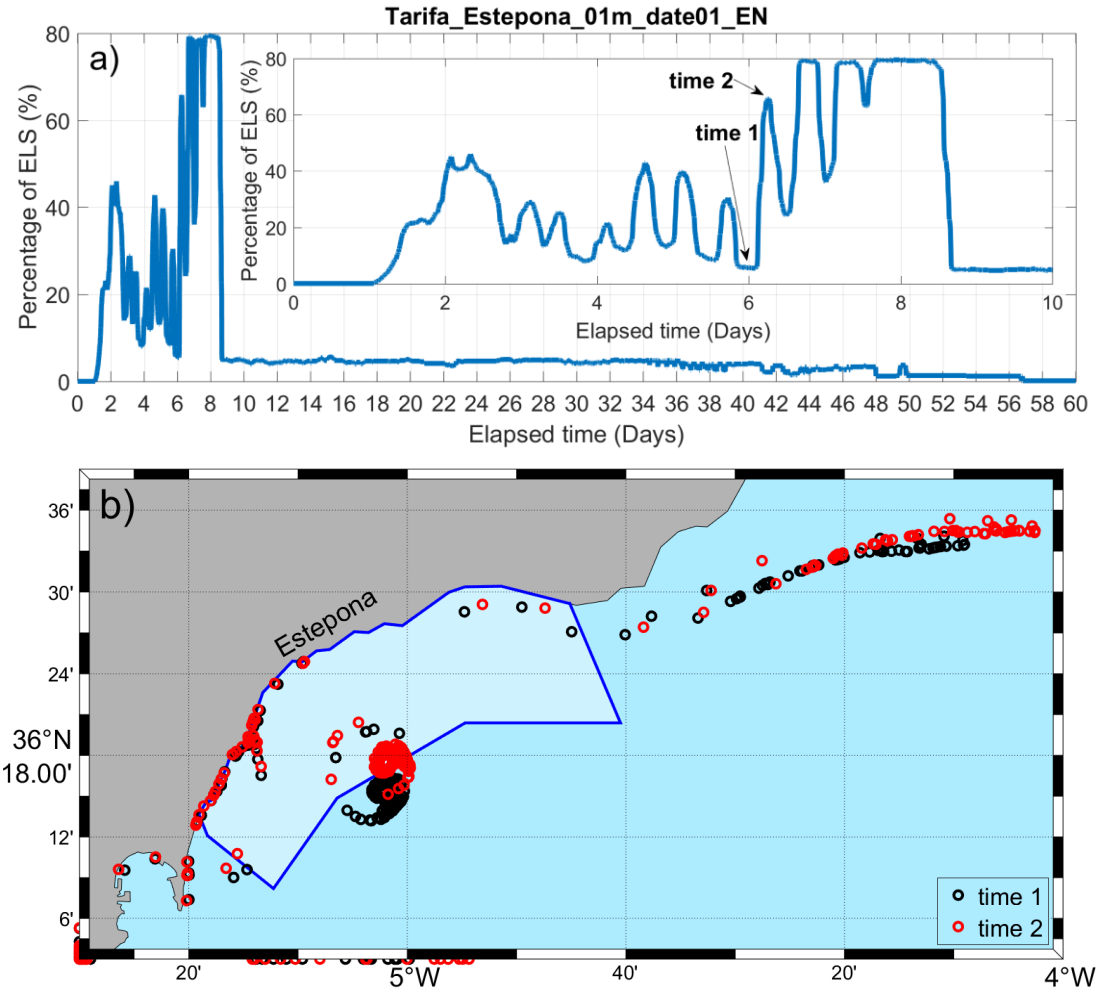

Figure 3 – Panel a): Time series of ELS concentration released in Tarifa area and collected in Estepona area (see Figure 2). The inset displays a zoom on the first 10 days. Panel b): Particles position at time 1 (black circles) and time 2 (red circles). The blue polygon delineates the Estepona area.

Later, at the end of day 8, particles leave definitely the Estepona area and follow moving eastwards, resulting in a quick drop of abundance, which remain at minimum values through the rest of the experiment.

This example, roughly applicable to almost the totality of the experiments, shades a light on the high short-term variability of the system in the Strait of Gibraltar – Alboran Sea region, and force

to pay special attention on the approach used to quantify the connectivity among the areas analyzed in this study. Although connectivity is typically computed at fixed time interval (Koszalka et al., 2009), this approach could provide unreliable results in this framework. A blind choice of 6 days, for instance, in this case would have led to a notable underestimation of the connectivity between Tarifa and Estepona areas, which instead present a much higher value only 6 hours later (Figure 3a). On the other hand, a higher time interval, closer to the PLD of the studied species (e.g.: 50 days), would have provided nearly null connectivity, notably underestimating the real connectivity between the analyzed zones, and completely neglecting the highly varying dynamics of the first days.

For this reason, the approach used in this study is to choice the maximum percentage of particles released in certain area and collected within a certain landing area, through the full 60-days simulation. Along with these percentages, also the times at which they have been reached is stored.

5. Results

For each of the 480 experiments, the connectivity between the release area and each of the 10 landing areas has been computed, resulting in a large multidimensional matrix C of 4800 elements:

$$C = A_r(3) \cdot T_p(4) \cdot T_s(2) \cdot D(5) \cdot R_p(4) \cdot A_l(10) \quad \textbf{1)}$$

Equation (1) shows the dependence of the connectivity matrix C of the:

- 3 areas of release (A_r): Tarifa, Tanger and TangerMED,
- 4 tidal phases (T_p): High, Ebb, Low and Flood,
- 2 tidal strength (T_s): Spring and Neap,
- 5 depths (D): 01 m, 12 m, 25 m, 52 m and 81 m,
- 4 replicas (R_p), see Figure 1,
- 10 landing areas (A_l): Cadiz, Estepona, Malaga, Roquetas, Carboneras, Arcila, Tetuan, Alhucemas, Melilla, Oran.

Such huge quantity of information has to be somehow summarized, and the general patterns for each of the analyzed zones (landing areas) have to be retrieved, along with their temporal and spatial variability.

Table 1 shows the averaged values of connectivity computed for all instances of T_p, T_s, D and R_p, for each pair of release-landing area.

As expected, the percentages of particles released in the Strait and collected inside the two landing areas of the Atlantic Ocean (Cadiz at north and Arcila at south) are nearly null in average. Westward (East-West) connectivity is strongly prevented by the eastward predominant current of the upper layers of the water column, at least up to the maximum depth analyzed in this study.

Table 1 – Averaged connectivity for each combination of release and landing area.

Landing area	Tarifa (%)	TangerMED (%)	Tanger (%)
Alhucemas	8±5	17±18	14±13
Estepona	38±11	8±8	10±6
Arcila	0±0	0±0	1±2
Malaga	45±12	11±8	15±7
Cadiz	0±0	0±0	0±0
Melilla	6±3	4±3	3±2
Oran	14±4	5±3	6±4
Tetuan	8±5	45±19	33±17
Carboneras	6±4	2±3	2±2
Roquetas	17±8	5±4	5±4

Tarifa

The northern coast of the main channel of the Strait (Tarifa area of release) is mainly connected with the northern coast of the Alboran basin, showing the three highest percentages in Malaga, Estepona and Roquetas, 45%, 38% and 17%, respectively, a clear consequence of the effect of the AJ and its prolongation along the northern rim of the WAG. In agreement with this result, the fourth highest value (14%), found in Oran, is the result of the presence of the Almeria-Oran front, a well-known dynamic structure at the eastern margin of the Alboran Sea, which connects the northern with the southern coast of this basin (Renault et al., 2012; Sánchez Garrido et al., 2013). Carbonera landing area lays at east of this front, being somewhat isolated from what occurs at west, and presents a quite lower percentage (6%). For what concerns the rest of the southern coast, Alhucemas and Tetuan present the same averaged percentage of 8%, sign of a clear east-west connectivity along the southern coast (the southern rim of the WAG), while Melilla report the lowest value in the Alboran basin, being highly dependent by the interaction of the two Alboran gyres and the sluggish circulation between them (see Figure 2 in the intermediate report).

TangerMED

The southern coast of the main channel of the Strait (TangerMED release area) presents the highest degree of connectivity with the southern coast of the Alboran basin, with values of 45% and 17% for Tetuan and Alhucemas landing areas, respectively. This is mostly due to two concomitant mechanisms acting at the same time, with relative intensity depending on the tidal strength and wind modulation: 1) a coastal (clockwise) gyre, smaller than typical size of WAG, moving closer to the Strait exit, and veering southwards, and 2) the higher occurrence of particles released in the southern coast of the Strait in the inner portion of the WAG, more prone to spread towards the southern coast of the basin. After Tetuan and Alhucemas, the landing areas presenting the highest percentages are Malaga and Estepona (11% and 8%, respectively), related again with the dynamics of the the WAG, which is also (secondarily) involved by particles released in TangerMED area. As occurred for Tarifa release area, Roquetas and Oran present the same percentages (5%), while Melilla and Carboneras lay quite isolated by the rest and show the lowest values (4% and 2%). As expected, Cadiz and Arcila show null connectivity (in average), also in this case.

Figure 4 shows results of a global simulation, in which approximately 1500 particles have been released through the whole Strait, every day during a week, for a total of 11000 elements. The snapshot, coding with colors the latitude of release, is particularly illustrative of all what has been discussed so far.

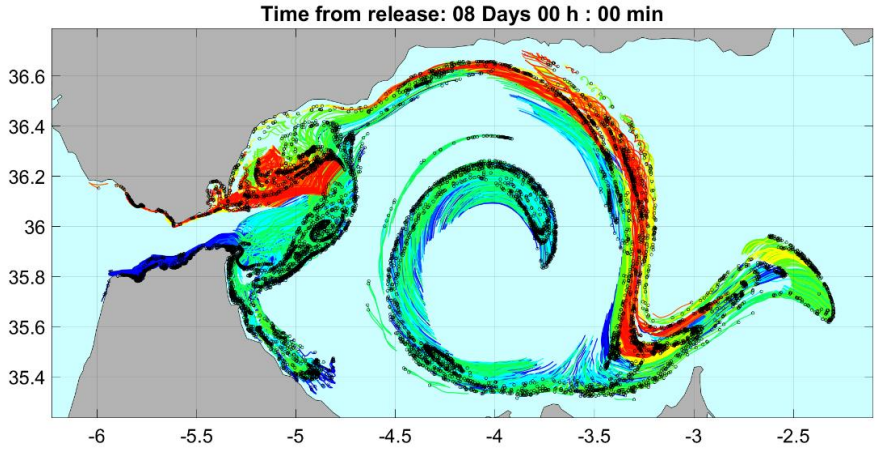

Figure 4 – Particles position 8 days after release of a total of 11000 units in the whole Strait. Colors indicate the latitude of the initial position, being bluish the southernmost ones and reddish the northernmost.

8 days after the first release, particles started in the central-southern portion of the Strait (blue-green) are mainly spread along the southern coast of the Alboran Sea. The coastal gyre generated at the very eastern Strait exit moves sluggishly along the coast of Tetuan, while the inner portion of the WAG spreads, more likely than its outer counterpart, along the southern coast of Alhucemas. Both results agree with the higher percentage observed in Tetuan area, which receives particles directly from the Strait, and the lower of Alhucemas area, which collects them only after a long route along the whole WAG (notice also the larger distance of particles from the coast of Alhucemas (see also Figure 2), with respect to Tetuan, which would partially explain the lower percentage observed). This discrepancy in terms of different connectivity paths of neighbor areas will be confirmed by the times recorded with the connectivity maxima, which will be discussed later.

Although most of particles released at the southern coast of the Strait are collected through the south of the Alboran Sea, a good portion of them have the chance to join the northern path of the WAG and spread along the northern coast (Malaga and Estepona).

Conversely, particles released along the northern coast of the Strait (red-yellow) spread almost totally along the northern margin of the Alboran Sea, and depicts clearly the Almeria-Oran front, hence explaining the high percentages found in Malaga, Estepona, Roquetas and Oran areas. Notice that particles at the very northeast exit of the Strait move northeastwards drawing the cyclonic eddies discussed in the intermediate report, and lay at certain distance of the coast of Estepona, likely explaining the lowest percentages of this area with respect to Malaga, which undergoes stronger and straighter currents. This issue will be related to the different scattering behavior of spring and neap tides, later in the text.

Tanger

The highest percentages for Tanger release area are found in Tetuan, Malaga, Alhucemas and Estepona, with 33%, 15%, 14% and 10%, respectively. Highest percentages recorded in Tetuan

are likely related to the Earth rotation effect, which foster particles to move more likely along the southern coast, resembling closer the results of TangerMED release area. Once more Roquetas and Oran share a very similar percentage (5% and 6%, respectively). The rest of landing areas of Alboran show very low percentages, while Arcila (at west of the release area) in this case shows a no-null connectivity.

Results reflect a sort of mixing of both previous cases (although a general higher similarity with TangerMED case), with generally lower connectivity, certainly due to the highest distance and the dynamic barrier of the Camarinal sill, located between the release area and the Alboran basin. ELS are expected to be roughly scattered before to join the strong and regular AJ advecting them eastwards, and its dispersion inside the Alboran Sea follows a fuzzier pattern, with less discrepancy between the northern and the southern coast of the basin.

So far, only the averaged percentages have been discussed, while much attention has to be paid to their uncertainties, generally very high (higher than the own mean in some cases), reflecting a high variability of the system. Temporal and spatial variability, at the origin of such uncertainty, will be discussed in detail in next sections.

5.1. Whole set of experiments

The next three panels summarize the full connectivity matrix for the three release areas analyzed in this study. Although hard to interpret singularly, the figures show both the general pattern described so far, and the spatial and temporal variability due to tidal phase, tidal intensity, and depth.

Few illustrative examples can be provided for the sake of clarity:

1. The highest connectivity for Tarifa release area is observed in Estepona landing area, with percentages close to 60% (of the same order of Malaga landing area). However, great variability is observed due to both tide and depth. In particular, the highest connectivity is observed in Ebb-Spring (ES) conditions (see Figure 5 → Estepona). During ebb tide, the eastward current is maximum in the Strait, and the ELS are advected directly to the Alboran Sea, with nearly no recirculation. Under spring tide, this circumstance is enhanced and the percentage of particles advected from Tarifa to Estepona is maximum. However, particles collected in Estepona do not land there directly from the Strait, but recirculate along the cyclonic eddies forming at the very northern exit. Size and spread of these eddies depend on the tidal intensity, being higher under spring tides, when particles arrivals along that coast are more likely. This feature is maximum at surface and decreases its intensity with depth.

2. Although connectivity for Malaga landing area (from Tarifa release area) is of the same order of magnitude of Estepona, which is expected on the other hand for their proximity, a notable difference exists in terms of tidal variability. In Malaga all the tidal phases under neap tide present systematically higher connectivity than their spring counterparts. Moreover, this issue seems to be enhanced with depth (see Figure 5 → Malaga). The higher energy available under spring tide, tends to scatter ELS more strongly, and indeed it provokes a lower rate of arrival of particles in Malaga than the one obtained under neap tide. The same figure repeats in the following landing areas along the northern coast (Roquetas and partially Carboneras) , confirming this issue (see

Figure 5). Actually the higher the distance, the higher the ELS scattering, and the lower the connectivity observed. This figure is similar (but contrary) to the one described at previous point. In Estepona the higher the scattering of particles, the higher the probability of ELS to fall within that landing area.

3. A similar circumstance is observed for TangerMED release area (see Figure 6). Besides the higher connectivity globally found along the southern coast of the Alboran basin, what is worth noting are the higher percentages found in all the tidal phases (especially at shallower depths) under spring tide in Tetuan landing area (see Figure 6 → Tetuan). This fact resembles the previous case of Tarifa-Estepona, where the higher ELS scattering is directly related to the size of the eddy (the anticyclonic coastal gyre at the very southern exit of the Strait, in this case), who enhances the arrival of ELS into the whole landing area of Tetuan. Even more peculiar is the huge discrepancy between the 25 m depth level and the other levels in Alhucemas landing area (see Figure 6 → Alhucemas). In this case, ELS do not come directly from the Strait, but travel along the whole WAG before to fall within this area, and do it with special efficiency at this depth. Too much energy and scattering for shallower depths and too low energy and higher distance from the coast for deeper ones.

4. As discussed before, Tanger release area is a mixture of both Tarifa and TangerMED areas. A similar behavior of high (low) connectivity under spring (neap) tide in Estepona/Tetuan (Malaga) landing areas is observed (see Figure 7), although with percentages much lower than in Tarifa case. The same spikes presented by the 25 m depth level of Alhucemas landing area found for TangerMED release area is observed here, reflecting the higher similarity with this area respect to Tarifa. What is a unique feature of this release area is the no-null connectivity with its Atlantic façade. While results for Cadiz landing area are anecdotic, particles advected westwards at the beginning of the simulation under low (LS and LN) or flood tide (FS and FN), have certain chance of being trapped along the Atlantic coast of Arcila (see Figure 7 → Arcila), and show few units of percentages, which are comparable with the most isolated areas of the Alboran basin (e.g.: Melilla, Carboneras). This occurs mainly at shallower depths, being zero the connectivity of 52m and 81m.

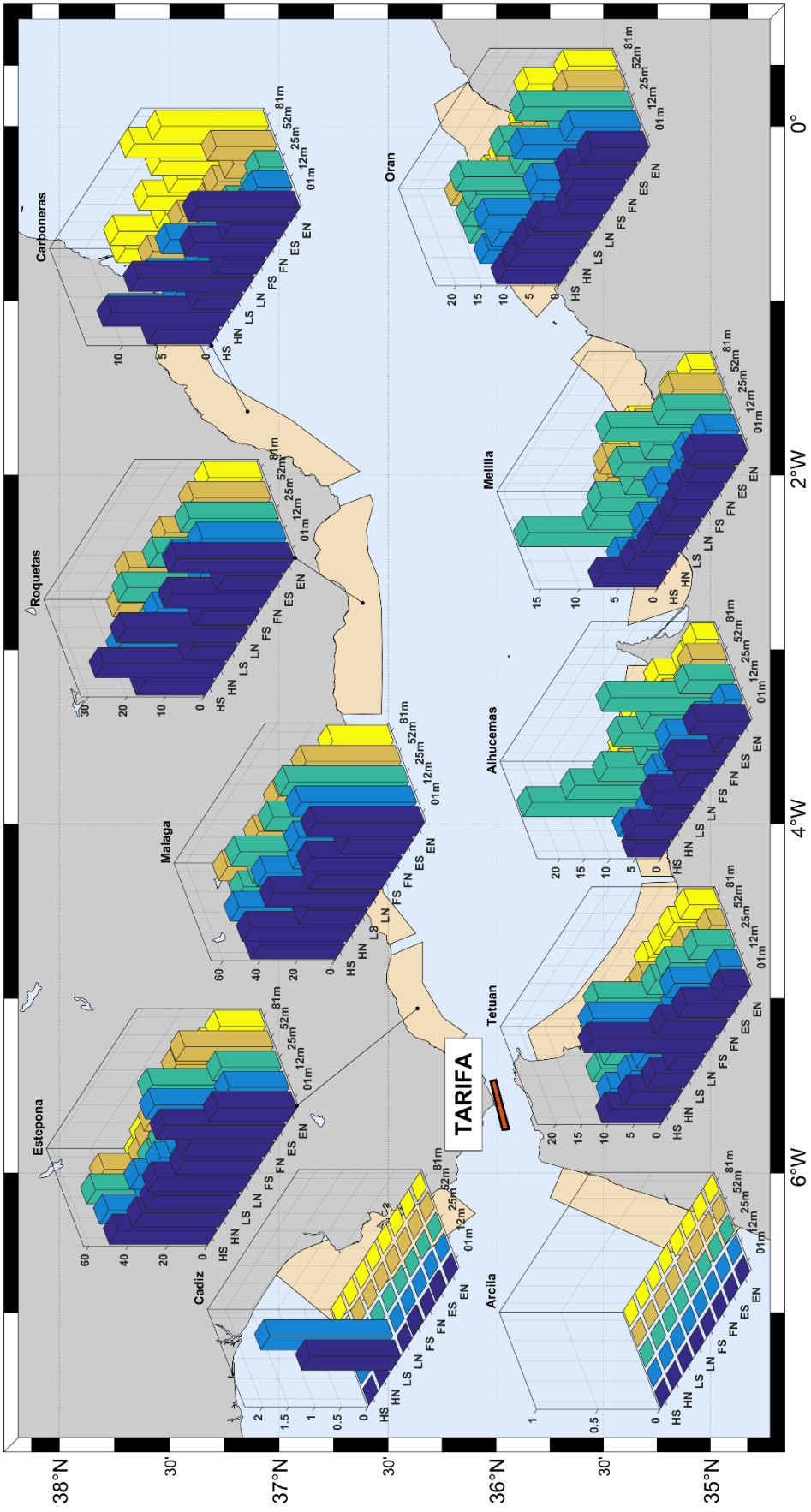

Figure 5 – Full connectivity results for Tarifa release area.

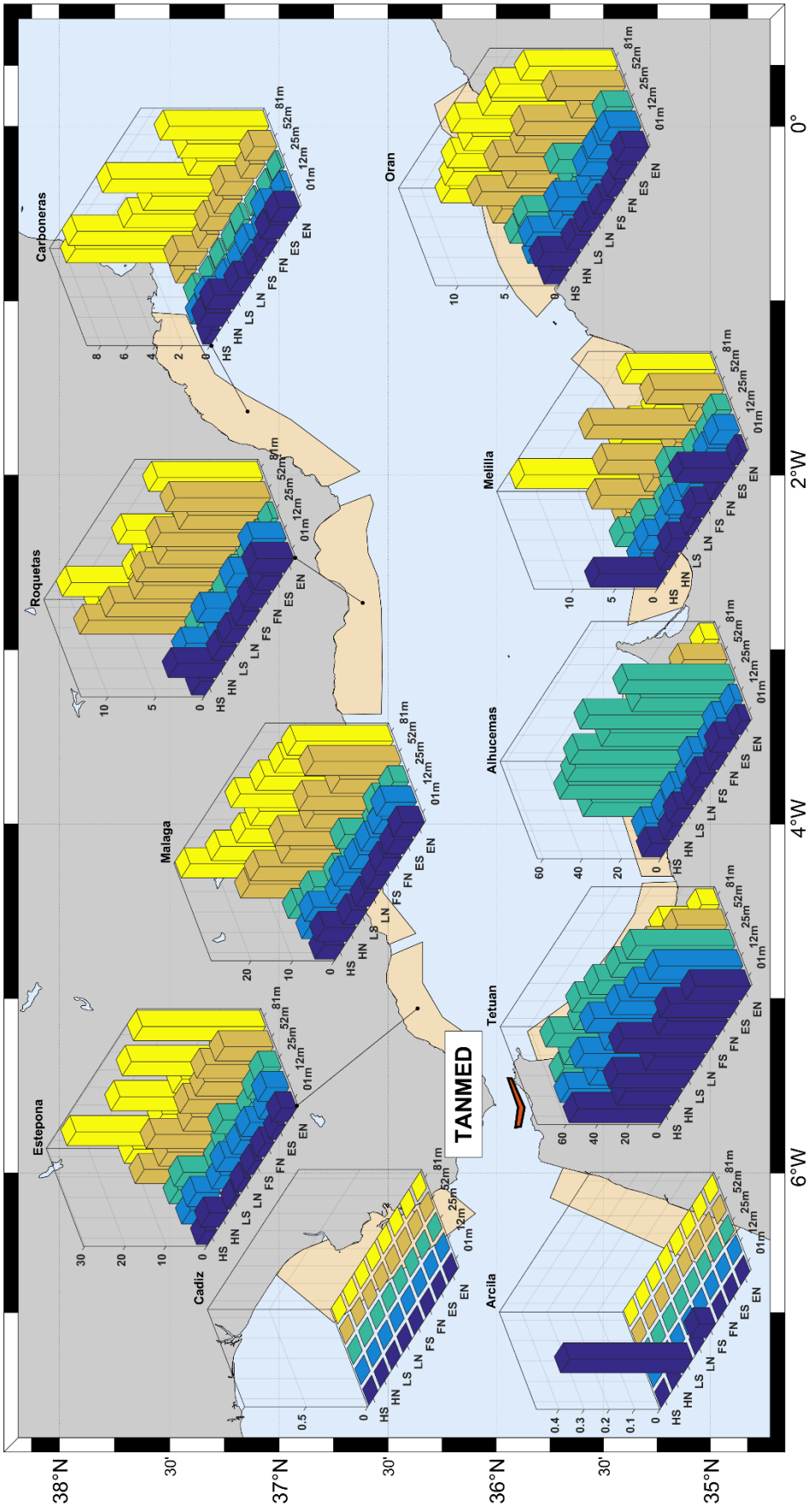

Figure 6 – Full connectivity results for TangerMED release area.

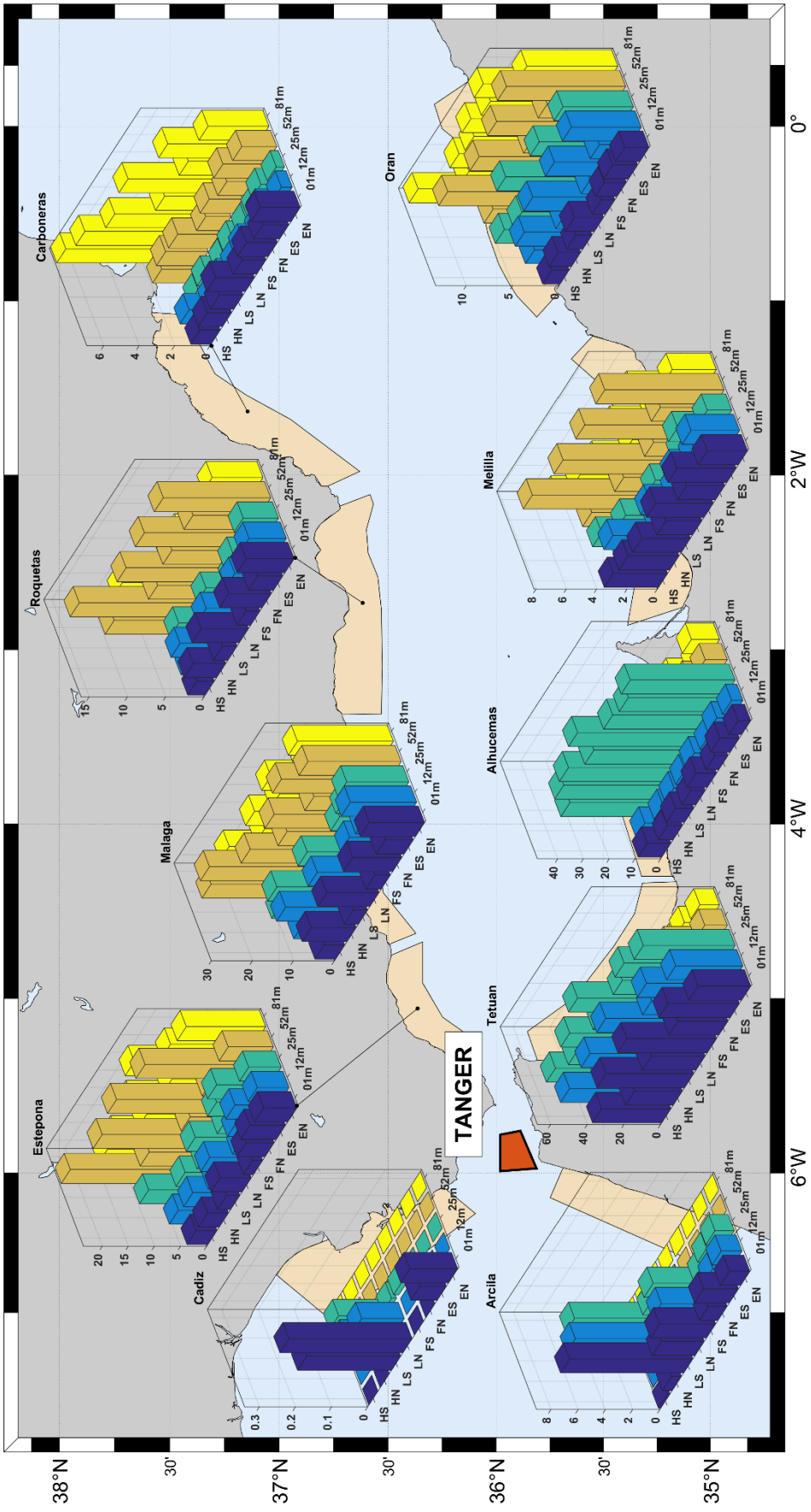

Figure 7 – Full connectivity results for Tanger release area.

5.2. Temporal variability

As discussed in the intermediate report, tides are one of the predominant factors in the water current modulation, both at the own tidal scale (semi-diurnal and diurnal periodicity) and at subinertial scale (fortnightly cycle). It is expected, therefore, that such variability was reflected on the ELS spreading patterns, and indeed the previous section provided few clear examples of it.

Figure 8 shows the time series of percentage of particles released in Tarifa and collected in Estepona area, during the four tide phases (high, low, flood and ebb) under spring tide, at surface. The pattern shown in the four cases is quite coherent, but a marked difference both in relative abundance and time of arrival exists. Both high and ebb tide show the highest percentages and the earliest time of arrival (day 1.3), with high tide almost doubling the values observed for ebb tide at the first peak. Later (around day 2) their peaks converge and the final difference of maxima is not as high as at the beginning (~81% and ~67% for high and ebb, respectively). After them, flood and low tides present the lowest percentages, with flood tide reaching the landing area slightly before than low, for its own dynamic functioning (during low tide, water flows westwards few hours more, before to invert, with respect to flood tide).

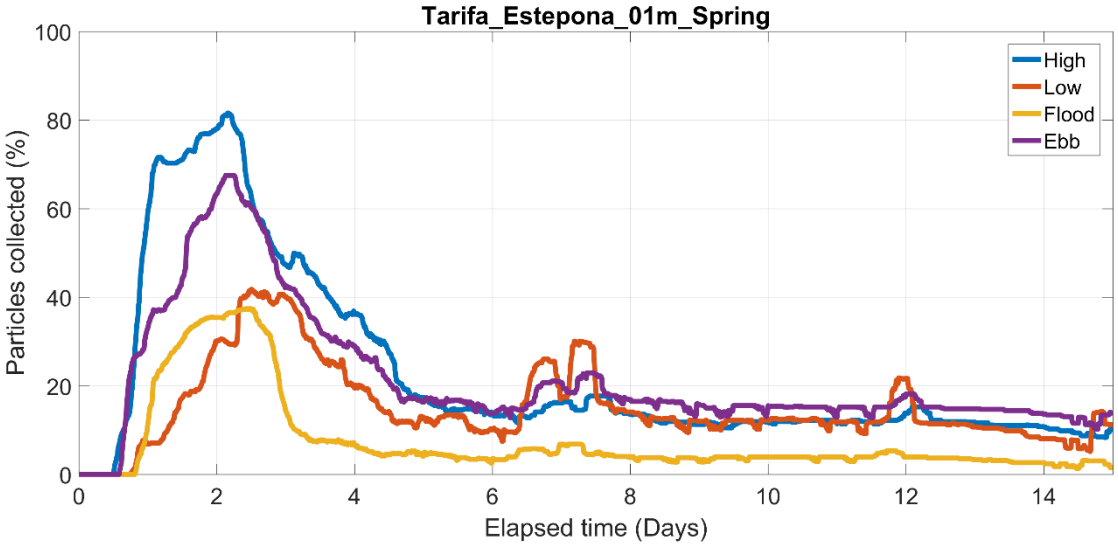

Figure 8 – Time series of percentages of particles released in Tarifa and collected in Estepona, under spring tide at surface.

Such apparently clear pattern is blurred by the other replicas of the same tidal conditions run in the other three periods (see Section 4.1), where these differences are not so evident. Actually, averaging the four replicas, the discrepancies among the tidal conditions vanish notably, letting the ebb tide (under spring tide) as the most connected (see Figure 5 → Estepona).

What is a much more constant result, throughout the replicas and the landing areas (at least the ones of the northern coast of the Alboran Sea), is the effect of the fortnightly tidal modulation (spring-neap tide cycle). Figure 9 shows the time series of percentages of particles released in Tarifa and collected in Malaga at surface, under the whole set of tidal combinations aforementioned. As commented before, under neap tide ELS are advected into the Malaga landing area in a more efficient way than under spring tide. Although with slightly difference among the tidal phases (surprisingly ebb and low tides present higher percentages than high

and flood, under neap tide), the time series obtained under neap tide show much higher percentages than spring tide.

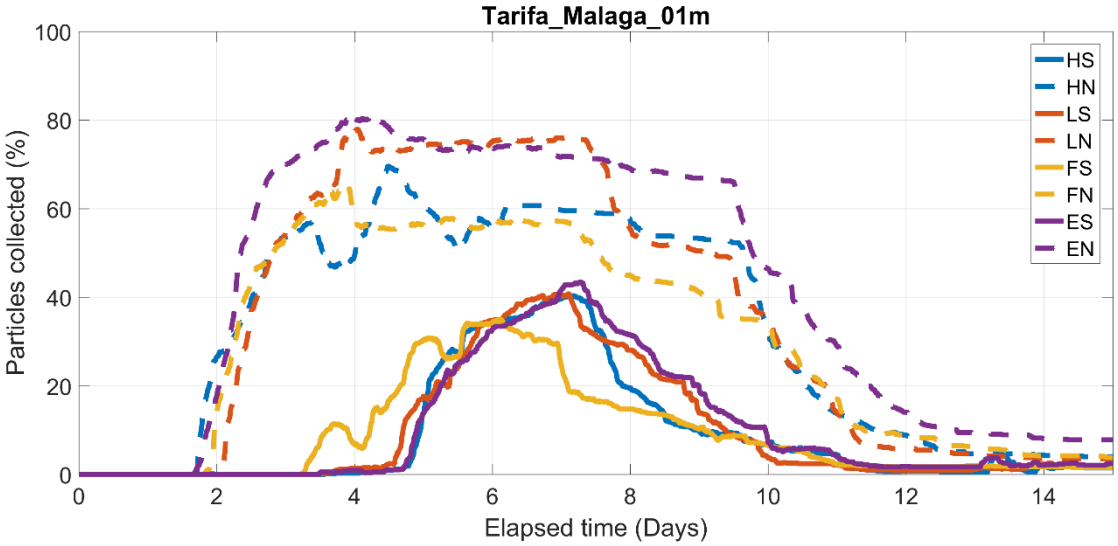

Figure 9 – Time series of percentages of particles released in Tarifa and collected in Malaga, at surface, under the 8 combinations of tidal forcing discussed in the text.

A very similar result can be obtained for the rest of the landing areas of the northern coast of Alboran Sea, which are not shown, for the sake of clarity.

The opposite occurs in Estepona area, where spring tide improves the arrival of ELS by enhancing the dynamics of the cyclonic eddies developing over the northwestern coast of the basin (Figure 10).

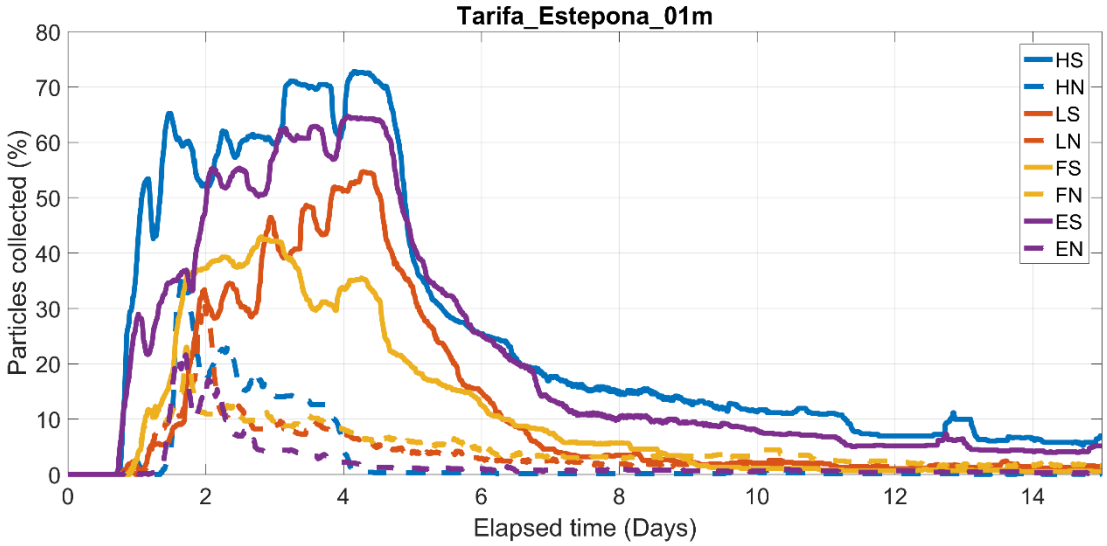

Figure 10 – As in Figure 9 for Estepona landing area.

Here spring tides present percentages few tens of points higher than neap tide, in average. Also notice the different order (in terms of percentages) of the tidal phases with respect to the case of Malaga. In the former the higher percentages were observed for ebb and low tide (under neap tide, see Figure 9), although their difference with the rest of tides was relatively low. Conversely, in the latter, the order is the one expected for an eastward current: high tide as the

one presenting the higher percentages, later ebb tide and then the others. Moreover, the differences among the tidal phases are quite higher in Estepona area than in Malaga: as a more energetic framework, spring tides enhance the tidal phase discrepancy (Estepona), with respect to neap ones (Malaga).

5.3. Spatial variability

A further degree of freedom to be analyzed is the spatial variability due to the choice of release depth. Figure 11 shows two replicas of the time series of percentages of particles released in Tarifa and collected in Estepona, under high-spring tide. All 5 depth levels are depicted.

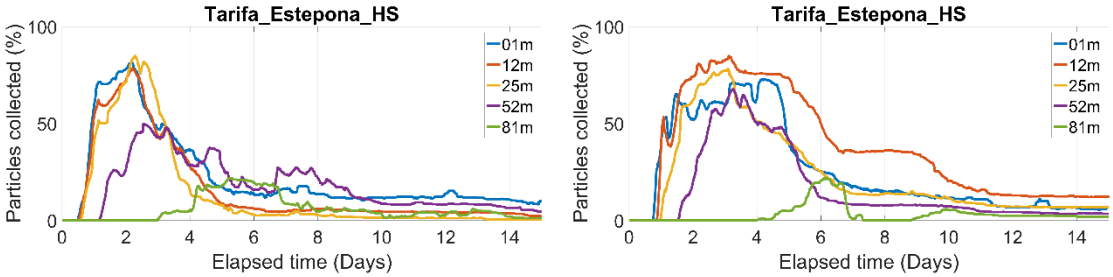

Figure 11 – Time series of percentages of particles released in Tarifa and collected in Estepona, under high-spring tide at the five depth levels discussed in the text. The left and right panel refer to two of the four replicas run.

The effect of depth seems to be harder to define, due to the high uncertainty presented by most of experiments. Although some kind of vertical structure is envisaged in these two examples (1 m, 12 m and 25 m seem to be quite different from 52 m and specially from 81 m), many of them, not shown here for the sake of clarity, present more discrepant results. After all, the first three levels are very close each other and it is expectable that their differences fall within the own uncertainty of the method.

The deepest depth levels (52 m and 81 m) are somewhat different and generally present the farthest levels of connectivity from the surface levels. In this case, their percentages are notably lower than the ones obtained for the shallower levels. Particles released in Tarifa are swiftly advected eastwards at surface, while they stay much more time moving back and forth within the own Strait before to enter the Alboran Sea, at deeper depths. When they finally exit, the weaker current is not able to scatter them enough to let them fall massively into the landing area of Estepona.

Figure 12 shows two opposite examples, in which the two deepest levels show the highest connectivity. Both of them refer to the case of TangerMED release area, and two landing areas of the northern coast of the Alboran basin (Malaga, and Roquetas).

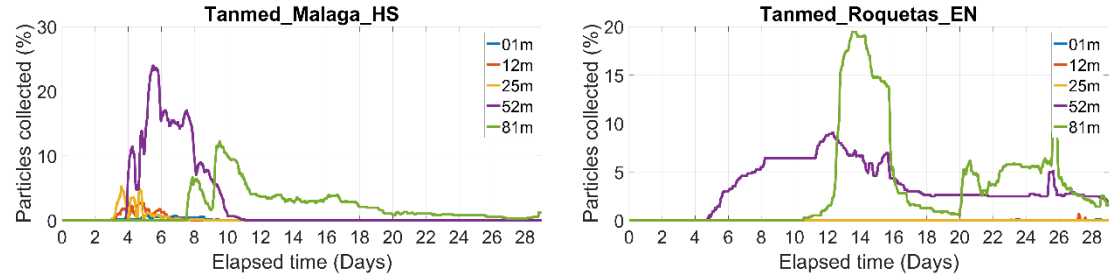

Figure 12 – Time series of percentages of particles released in TangerMED and collected in Malaga (left) and Roquetas (right), under high-spring (left) and ebb-neap (right) tide at the five depth levels discussed in the text.

In this case the discrepancy between the shallower levels and the deeper ones is due to the behavior of the particles at their exit from the Strait. At surface they are tightly trapped inside the coastal gyre moving along the southwestern Alboran coast, and preventing them to move northwards. Conversely, at higher depths the gyre is weaker and particles reach more efficiently the northern coast.

One further aspect worth mentioning is the marked discrepancy between the percentages observed in all tidal conditions for the 25 m depth level and the rest of depths, for all release areas and specially for TangerMED one, at Alhucemas landing area. Figure 13 shows the time series of percentages of particles released in TangerMED and collected in Alhucemas, at all the 5 depth levels, and the trajectories of the levels 25 m and 1 m, recorded 52 days after the release (within the peak shown by the 25 m depth curve – panel a).

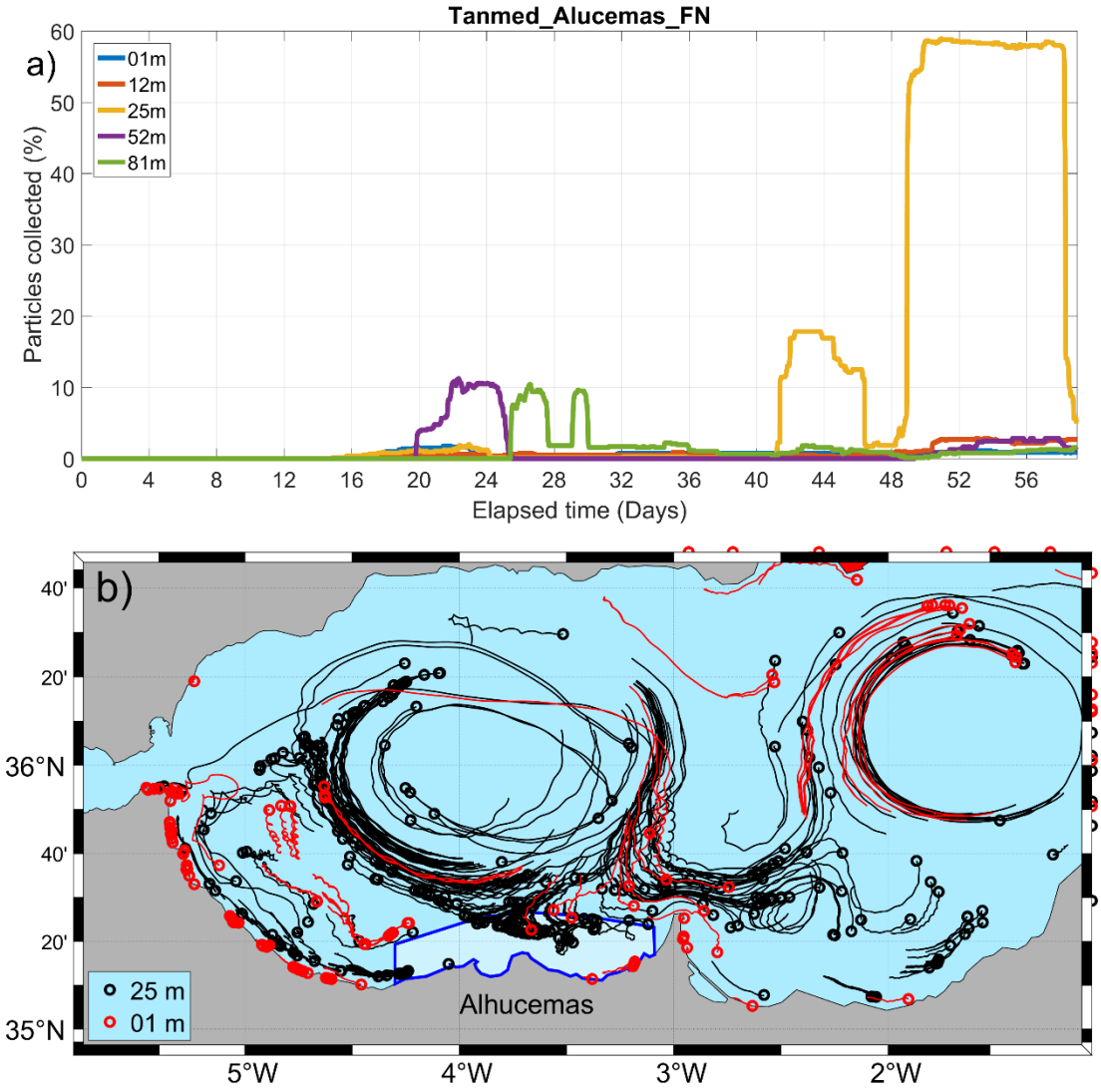

Figure 13 – Panel a): Time series of percentages of particles released in TangerMED and collected in Alhucemas, under flood-neap tide at the five depth levels discussed in the text. Panel b): 5 days-length trajectories of the Lagrangian simulation depicted in panel a), performed at 25 m depth (in black) and 1 m (in red), 52 days after the release.

As suggested by the Alhucemas plot in Figure 6, this landing area collects particles principally at the depth level of 25 m, while the other levels show percentages some tents of points lower.

Figure 13a reflects this issue presenting for the depth level of 25 m a first peak of approximately 18% around day 41, lasting 5 days, and a second much higher peak of approximately 60% starting at day 39 and lasting 9 days. The shallower levels present nearly null connectivity. Figure 13b gives a hint on the mechanism at the origin of this result: particles at 25 m depth travel along the whole WAG before to reach Alhucemas landing area (first peak is observed at day 41), and then do it massively. On the contrary, surface particles veer southwards just after their exiting from the Strait, they fill the Tetuan area (see Tetuan plot in Figure 6) and end flowing sluggishly along that coast without attaining Alhucemas.

5.4. Time of maximum connectivity

As mentioned before, for each maximum percentage computed, corresponds a time at which it is observed, which provides further information to properly interpret the connectivity patterns of the target species. Figure 14 shows two scatter plots of time vs. connectivity of all the tidal conditions for Tarifa and TangerMED release area, computed at 25 m depth.

For Tarifa release area (Figure 14a) Estepona and Malaga landing areas provide the highest connectivity at earlier times (2-4 days approximately), both under spring (squares) and neap (circles) tides for Malaga, and only under spring tide for Estepona. This reflects the poor chance of particles to be scattered shoreward in lower-energy neap tides. Under spring tides, instead, the AJ is more energetically spread when it exits from the Strait channel, and certain probability of turning southwards to the African coast is provided. Actually, Tetuan presents lower but no null connectivity at a time comparable to the one observed for the northern coast, sign of a simultaneous mechanism feeding both sides of the basin. Results for Alhucemas landing areas are related to the dynamics of the WAG. A weaker, smaller and less spread WAG under neap tide, advects particles to that area in a shorter time (around 20-30 days), while a larger and swifter gyre more prone to follow flowing eastwards, have little chance to reach the southern coast, doing it barely and very later. In both cases, connectivity with the southeastern African coast is much limited because of the release area located over the northern Strait. A worth noting issue is the scarce connectivity observed in Tetuan area under neap tide conditions, whose values follow in time the ones observed in Alhucema area during the same conditions. A closer look reveals that while short-time values observed in Tetuan area under spring tides are the result of a direct connection with the Strait (eastward connectivity), the longer-time ones, obtained under neap tide, proceed from the Alhucema and reflect a westward connectivity.

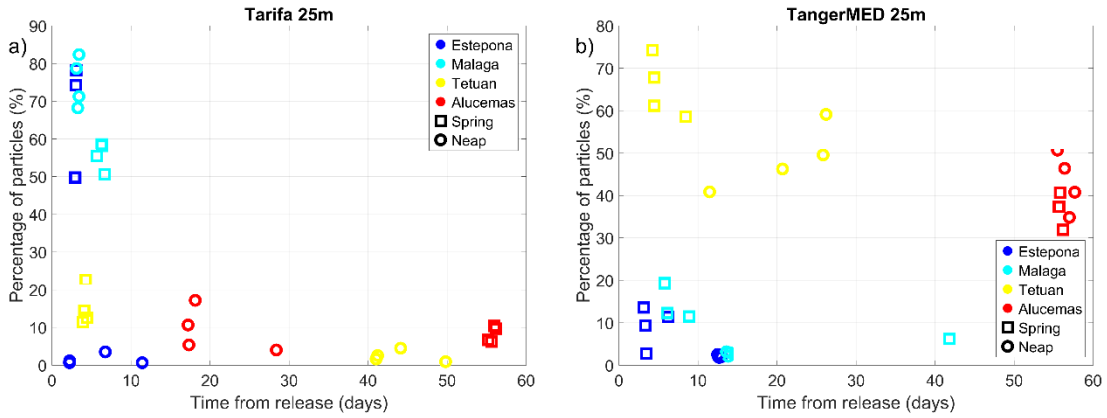

Figure 14 – Scatter plots of percentages of particles released in Tarifa (panel a) and TangerMED (panel b) vs times of arrival, at 25 m depth. See legend for interpretation of tidal conditions.

Results from TangerMED release area (Figure 14b) present a completely opposite situation. Tetuan area is the one presenting the highest connectivity, directly from the Strait exit, at earlier (later) times under spring (neap) tides. Alhucemas receive particles both from the own Tetuan area under spring tides and from the WAG under neap tides. In both cases, maxima are attained at very later times. Estepona and Malaga present certain degree of connectivity under spring tides, thanks to the spread of the AJ at its exit, and actually coincide in times with the corresponding maxima obtained for Tetuan area. Under neap tides their chances to be reached by some filaments detached by the main coastal gyre are very scarce, and connectivity under these tidal conditions is nearly null.

6. Conclusions

On the light of what discussed so far it is possible to sketch some general connectivity patterns of the Strait – Alboran Sea system for the target species.

The northern coast of the Strait (Figure 15) is strongly connected with the northern margin of the Alboran Sea, thanks to the straight connection of the AJ and the northern rim of the WAG, which flows swiftly along the northern margin of the basin.

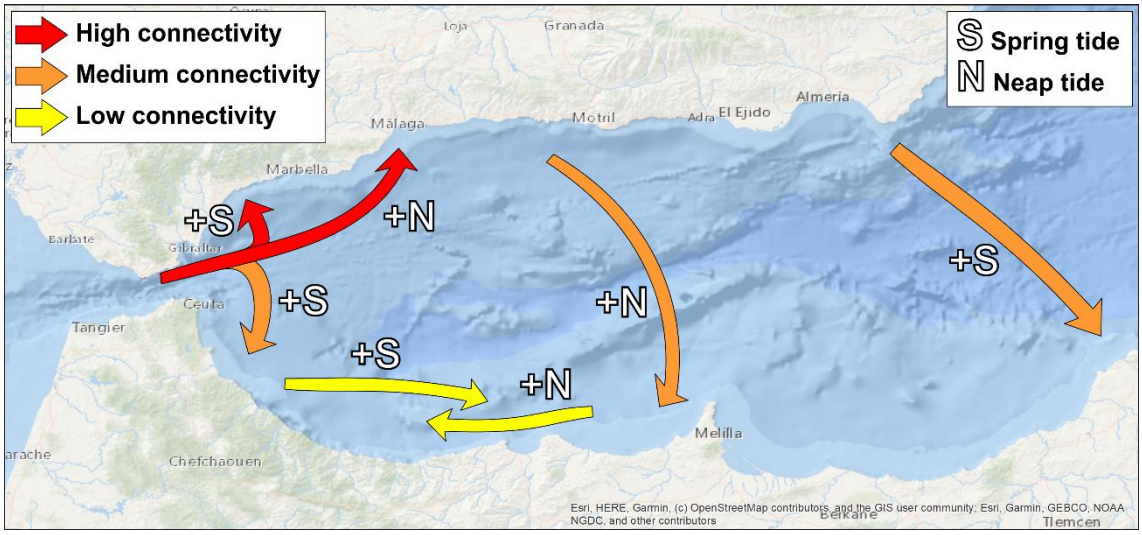

Figure 15 – Sketch of the connectivity patterns between the northern coast of the Strait and the Alboran Sea.

Spread of ELS in the Estepona coastal area is especially enhanced by spring tides, which promote the broadening of the cyclonic eddies generating along the northern rim of the WAG, and the corresponding increase of their range of action. For the same reason, the rest of the northern coast is mostly reached under neap tides, which spread particles less, and allow them to reach farthest distances. When WAG reaches its eastern margin, it splits in two directions: 1) eastwards, feeding the rest of the structures in this part of the basin (the Eastern Alboran Gyre and the Almeria-Oran front), and 2) southwards closing the gyre and veering westwards. Eastward connectivity is therefore enhanced under spring tides, while southward one is mostly fostered by neap tides. Under spring tides the higher spread of the AJ at its exit promotes the formation of a southern coastal gyre which feeds the southern coast directly, and gives origin to a much quicker and more efficient connectivity of the northern Strait to the African coast. Under neap tide, this mechanism is notably reduced: ELS are generally confined along the westernmost part of the African coast, and only under spring tides they are sluggishly advected eastwards. In this framework, then, ELS that reach the easternmost portion of the southern coast proceed

from west. Conversely, under neap tides, the connection along the southern coast is mostly westwards, where ELS moving there proceed mostly from east. In both cases, times for ELS spreading along the southern coast are long, especially for the second mechanism, occurring under the action of weaker currents.

Connectivity with the southern margin of the Strait (Figure 16) follows quite different patterns although it shares some specific advection scheme with the northern counterpart.

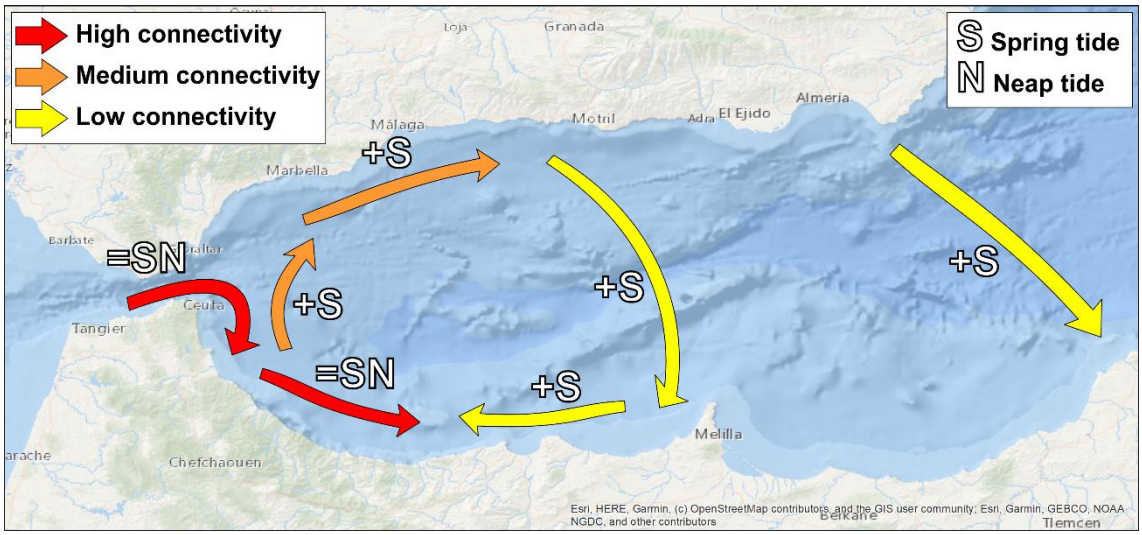

Figure 16 – Sketch of the connectivity patterns between the southern coast of the Strait and the Alboran Sea.

The main mechanism acting for ELS coming from the southern margin of the Strait is to involve them into the rather permanent coastal gyre forming at the very southern exit of the Strait. Almost regardless the spring intensity modulation, ELS are swiftly advected southwards and flow along the whole African coast featuring eastward connectivity. Spring tides give origin to the only case of northward connectivity in the basin. When the coastal gyre is especially wide and strong (under spring tides) the probability that the most external portion of it detaches and starts flowing northeastwards is quite high. ELS, initially destined to the African coast have the chance of being spread along the northern coast. When it occurs, ELS are able to follow the WAG pathway and spread both eastwards and southwards, feeding the African coast with a less efficient westward connectivity.

Although the sketches drawn so far can be reasonably assumed as valid for most of situations, it is clear that depth and subinertial variability, especially of meteorological nature, can easily turn the tables.

Generally speaking, depth fosters the farthest connectivity. The higher the depth, the weaker and especially the more stable the current. This helps to limit the ELS scattering along longer pathways and hence enhance the connection among farther sites. This can be observed for all the three release areas.

On the other hand, a strong atmospheric pressure gradient between the Atlantic and the Mediterranean sides of the Strait can accelerate or slow down the AJ (García Lafuente et al., 2002; Renault et al., 2012), with a corresponding enhancing or dropping of the WAG structure, of the cyclonic eddies along the northern Alboran coast, or of the coastal gyre along the southern one. Also, the evolution of the structure of the WAG observed in the intermediate report (see Figure 2 therein), with its progressive consolidation along the months, affect the whole

circulation scheme in the basin. The coastal gyre promoting connectivity from the Strait and the African coast (especially from the southern coast of the Strait) is progressively weakened with the corresponding strengthening of the WAG, and such type of connectivity is correspondingly reduced.

All these sources of variability likely overcome the expected interannual variability of the Strait of Gibraltar – Alboran Sea circulation, especially if we take into account that winter – spring period shows the highest degree of unpredictability of the system. It is very likely that the expected discrepancy between the results coming from the repetition of this study over further years, and the ones obtained by this one, could be masked by the own system variability. Therefore, further studies may not worth the huge work made in the present one.

Acknowledgements

I want to warmly thanks my colleague José Carlos Sánchez Garrido, for his inestimable support and solid aid during the implementation of the hydrodynamical model, my other colleague Irene Nadal Arizo, for her tireless help on the run of the hundreds of Lagrangian experiments used in this study, and, least but not last, my colleague / chief Jesús García Lafuente, for his consultations and warm support during the progress of the work.

References

Báez, J.C., Macías, D., Castro, M. De, Gómez–Gesteira, M., Gimeno, L., Real, R., 2014. Assessing the response of exploited marine populations in a context of rapid climate change: the case of blackspot seabream from the Strait of Gibraltar. Anim. Biodivers. Conserv. 37, 35–47. https://doi.org/278389

Burgos, C., Gil, J., del Olmo, L.A., 2013. The Spanish blackspot seabream (Pagellus bogaraveo) fishery in the Strait of Gibraltar: spatial distribution and fishing effort derived from a small-scale GPRS/GSM based fisheries vessel monitoring system. Aquat. Living Resour. 26, 399–407. https://doi.org/10.1051/alr/2013068

García-Lafuente, J., Sammartino, S., Sánchez-Garrido, J.C., Naranjo, C., 2018. Asymmetric Baroclinic Response to Tidal Forcing Along the Main Sill of the Strait of Gibraltar Inferred from Mooring Observations BT - The Ocean in Motion: Circulation, Waves, Polar Oceanography, in: Velarde, M.G., Tarakanov, R.Y., Marchenko, A. V (Eds.), . Springer International Publishing, Cham, pp. 193–210. https://doi.org/10.1007/978-3-319-71934-4_14

García Lafuente, J., Delgado, J., Criado, F., 2002. Inflow interruption by meteorological forcing in the Strait of Gibraltar. Geophys. Res. Lett. 29, 20-1-20–4. https://doi.org/10.1029/2002GL015446

Gil Herrera, J., 2006. Biología y pesca del voraz [Pagellus bogaraveo (Brünnich, 1768)] en el Estrecho de Gibraltar. University of Cádiz.

Gil, J., Sobrino, I., 2002. Studies on Reproductive Biology of the Red (Blackspot) Seabream [Pagellus bogaraveo (Brünnich, 1768)] from the Strait of Gibraltar (ICES IXa/SW Spain), in: Scientific Council Meeting - September 2002.

Koszalka, I., LaCasce, J.H., Orvik, K.A., 2009. Relative dispersion in the Nordic Seas. J. Mar. Res. 67, 411–433. https://doi.org/10.1357/002224009790741102

LaCasce, J.H., 2008. Statistics from Lagrangian observations. Prog. Oceanogr. 77, 1–29. https://doi.org/http://dx.doi.org/10.1016/j.pocean.2008.02.002

Renault, L., Oguz, T., Pascual, A., Vizoso, G., Tintore, J., 2012. Surface circulation in the Alborán Sea (western Mediterranean) inferred from remotely sensed data. J. Geophys. Res. Ocean. 117. https://doi.org/10.1029/2011JC007659

Sánchez Garrido, J.C., García Lafuente, J., Álvarez Fanjul, E., Sotillo, M.G., de los Santos, F.J., 2013. What does cause the collapse of the Western Alboran Gyre? Results of an operational ocean model. Prog. Oceanogr. 116, 142–153. https://doi.org/http://dx.doi.org/10.1016/j.pocean.2013.07.002

Wesson, J.C., Gregg, M.C., 1994. Mixing at Camarinal Sill in the Strait of Gibraltar. J. Geophys. Res. Ocean. 99, 9847–9878. https://doi.org/10.1029/94JC00256